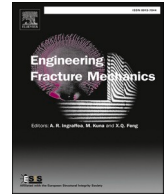




ELSEVIER

Contents lists available at ScienceDirect

Engineering Fracture Mechanics

journal homepage: www.elsevier.com/locate/engfracmech

Prediction of thermal shock induced cracking in multi-material ceramics using a stress-energy criterion

Roman Papšík^a, Oldřich Ševeček^b, Josef Schlacher^a, Raúl Bermejo^{a,*}

^a Department of Materials Science, Montanuniversität Leoben, Franz Josef-Straße 18, 8700 Leoben, Austria

^b Institute of Solid Mechanics, Mechatronics and Biomechanics, Faculty of Mechanical Engineering, Brno University of Technology, Technická 2, 616 69 Brno, Czech Republic

ARTICLE INFO

Keywords:

Thermal shock
Ceramics
Alumina
Multi-material
Coupled criterion
Finite fracture mechanics

ABSTRACT

Impact of residual stresses on the thermal shock resistance of alumina–zirconia multi-layer ceramics is investigated within the framework of finite fracture mechanics, using a stress-energy criterion. The critical temperature difference (ΔT_c) for crack formation is strongly dependent on the magnitude of residual stress and the material's strength. The predicted minimal spacing between cracks, critical time for crack initiation, and initial depth of the induced cracks are compared and discussed for different designs. An increase of up to $\sim 40\%$ in ΔT_c is predicted for multi-material ceramics with a thin alumina surface layer with compressive stresses, compared to bulk reference alumina.

1. Introduction

Ceramics are particularly prone to fracture when exposed to rapid and extreme temperature changes, a phenomenon known as thermal shock. This susceptibility is associated with their inherent brittleness, high elastic modulus and low thermal conductivity. Large gradients of temperature in a specimen occur when the resistance to heat conduction inside the body is much lower than the resistance to convection at the surface. Consequently, different thermal strains arise and tensile thermal stresses resulting from constrained deformation may lead to crack formation and fracture [1].

Crack initiation typically occurs above a critical temperature difference that depends on specimen's material geometry, properties and the quenching medium. Periodic arrays of crack are commonly observed in constrained specimens such as bars or rods, whereas networks of cracks may be found on unconstrained surfaces of discs, plates or balls. The spacing between cracks is influenced by the severity of the thermal shock. Since the fracture during thermal shock cannot usually be observed directly, the presence of crack is detected post-mortem, either using a dye penetration test or indirectly by evaluating the “retained strength” (i.e. strength after thermal shock).

The strength of fine grain ceramics tends to drop instantaneously above critical temperature difference ΔT_c [2–3], whereas for coarse grain ceramic the decrease is gradual [4]. Similar observations have been made also for glasses [5]. The decrease of strength is typically used as a measure of thermal shock severity. The retained strength is governed by initiated cracks of a given length and has a plateau above ΔT_c , which is explained by a transition from unstable to stable crack growth [6].

When the cracking is constrained, like bars or disc stacked together, a periodic array of uniformly-spaced cracks may be observed [7–9]. As the temperature difference increases, secondary or tertiary arrays of smaller cracks emerge [10–11]. When two arrays of cracks

* Corresponding author.

<https://doi.org/10.1016/j.engfracmech.2024.110121>

Received 26 February 2024; Received in revised form 11 April 2024; Accepted 27 April 2024

Available online 28 April 2024

0013-7944/© 2024 The Author(s). Published by Elsevier Ltd. This is an open access article under the CC BY license (<http://creativecommons.org/licenses/by/4.0/>).

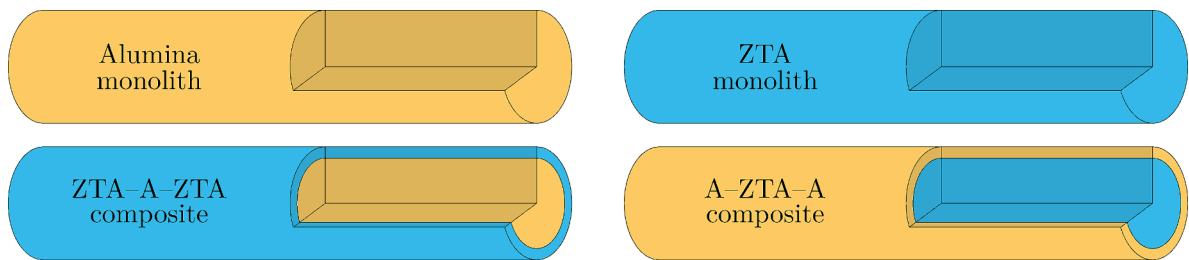


Fig. 1. Rod designs: Alumina and ZTA monoliths (top) and bi-material core-shell composites (bottom). All rods have an aspect ratio of length to diameter equal to 10 (50 mm to 5 mm) and the surface shell thickness of composite rods is 400 μm .

form, the longer cracks continue to grow after shorter cracks have stopped [12], phenomenon which has been experimentally demonstrated using a high-speed camera [13 14]. The crack spacing has an influence on the crack lengths [15 16] and on the retained strength as well [17].

The typical approach used for modelling of brittle fracture, the classical linear elastic fracture mechanics (LEFM), requires presence of a crack and is henceforth unable to predict crack initiation. In contrast, the finite fracture mechanics (FFM) approach [18 19] does not need presence of cracks and considers crack nucleation as a spontaneous fracture event, which allows predicting its initiation. The LEFM postulates that the propagation of a crack within material takes place once the Griffith-Irwin criterion (the energy release rate, G , reaches the fracture energy of the material, G_c) is fulfilled. However, initiation of cracks according to the FFM is governed by a stress-energy criterion, also called coupled criterion (CC), which states that the crack nucleation shall occur when both incremental energy release rate, G_{inc} , and the normal stress, σ_z , along the prospective crack reach respectively the fracture energy, G_c , and tensile strength, σ_c , of the material, simultaneously [20].

The coupled criterion has been employed in a variety of situations, for instance V-notches [20], plates with holes [21], particle debonding [22], fibre debonding [23], woven composites [24], transverse cracking [25 26 27], edge cracking [28 27], thin films [29] and coatings [30], indentation-induced ring cracks [31 32 33], dynamic fracture [34 35], penny-shaped cracks [36] and fracture at micro-scale [37 38 39 40]. We refer the reader to [19] and [41] for more examples. There are also other methods, alternative to the LEFM, that were used for modelling of the thermal shock fracture: The constrained cracking observed in [12] has been reproduced by simulations that include a non-local fracture model [42], damage models [43 44] and peri-dynamic models [45 46]. A representative volume element (RVE) is often used [47 48] with the coupled criterion [20] being employed to model crack initiation [49] and other fracture criteria to analyse crack propagation [50 51]. The use of the phase field models has also become a prominent tool to describe crack development in brittle materials [52 53 54 55].

The coupled criterion is to be applied in this study for the thermal shock simulations. In an attempt to correlate thermal shock crack formation with defect distributions in ceramics, Weibull statistics [56 57] has been employed [58], for instance to describe thermal shock in ceramic balls [59]. The probability of failure under an external applied stress in ceramics is often correlated to an underlying defect size density function, describing the number and size of potential critical flaws in the loaded volume. Two important parameters may be estimated, namely the Weibull modulus, m , and the characteristic strength, σ_0 for a reference volume V_0 . Since large specimens contain larger quantity of potential critical defects, its failure probability is higher than that of a smaller specimen at the same applied stress. This is called “volume effect” in the Weibull theory and must be taken into account when the strength distribution of different geometries is to be compared. Although some works have employed Weibull statistics to model thermal shock fatigue [60] and thermal shock with pre-made indentation cracks [61], the presence of strong stress gradients (as in thermal shock) makes this approach not suitable to describe crack initiation.

From the materials perspective, an interesting approach to enhance the resistance to crack initiation in ceramics is to design with compressive residual stresses (as utilized in strengthened glass through ion-exchange processes [62]). A recent investigation on ceramic laminates has shown the significant effect of surface compressive stress on the initiation of cracks through a (Hertzian) contact damage [63], which was modelled using the coupled criterion [64]. The effect of residual stresses on the thermal shock was experimentally investigated using bi-material laminates that consists of alumina combined with zirconia-toughened alumina [65 66 67 68], and has been also recently simulated using a phase field model [69]. An alternative approach, with ceramic compressive layers embedded in the structure, can also be very effective in retaining the propagation of surface cracks, as has been recently demonstrated on thermal shock experiments in 3D-printed ceramic components [70].

The aim of this work is to predict crack initiation in bi-material ceramic rods and to analyse the effect of surface compressive (or tensile) stresses during thermal shock, as compared to bulk ceramic counterparts. It is hypothesized that the shielding effect of compressive stresses should manifest itself by change of the critical temperature difference and the spacing of cracks. The effect of materials properties such as strength and toughness on the thermal shock response of the ceramic rods predicted by the coupled criterion will be discussed.

Table 1
Material properties of alumina (A) and zirconia-toughened alumina (ZTA).

Property	Unit	Alumina (A)	Zirconia-toughened alumina (ZTA)
Young modulus E	GPa	367 ± 9	333 ± 7
Poisson ratio ν	–	0.22	0.22
Density ρ	kg m ⁻³	3787	4345
Thermal conductivity κ	W m ⁻¹ K ⁻¹	34	22
Specific heat capacity c_p	J kg ⁻¹ K ⁻¹	880	665
Thermal expansion coeff. $\bar{\alpha}$	K ⁻¹	8.35 × 10 ⁻⁶	8.95 × 10 ⁻⁶
Fracture toughness K_{Ic}	MPa m ^{1/2}	3.1 ± 0.2	4.0 ± 0.1
Weibull modulus m	–	13.6 [10.2 – 16.6]	5.3 [4.0 – 6.4]
Char. strength σ_0 (biaxial bending)	MPa	645 [630 – 662]	1025 [962 – 1092]
Char. strength σ_0 (tension)	MPa	≈ 370	≈ 315

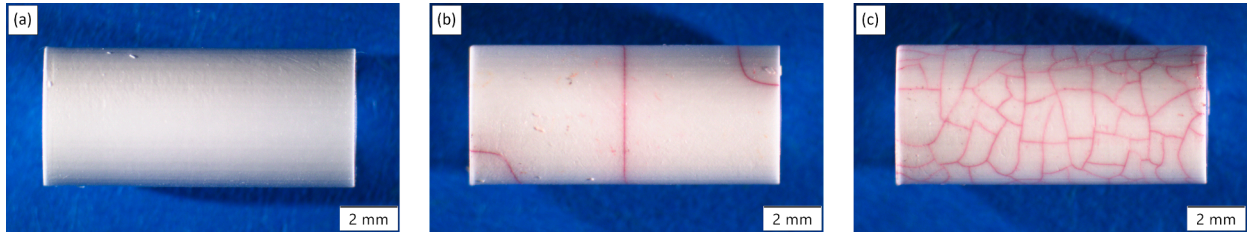


Fig. 2. Images of 3D-printed ZTA rods: (a) non-shocked and thermal shocked at (b) $\Delta T_0 = 250$ °C and (c) $\Delta T_0 = 400$ °C.

2. Experimental section

2.1. Materials and specimens

Two architectures, (a) monolithic cylinder and (b) bi-material cylinder with the core and the surface shell made of different materials, were studied (Fig. 1). The materials chosen for the thermal shock simulation were (i) pure alumina (named as A) and (ii) an alumina toughened by 20 vol.% of tetragonal zirconia (referred to as ZTA). The bi-material architecture containing two materials with different thermal expansion coefficient shall result in an unequal shrinkage, leading to residual stresses after cooling down from the sintering temperature.

The combined effect of residual stresses and thermal shock stresses caused by temperature gradients requires a knowledge of the stress-free temperature, which was determined to be approximately 1470 °C for the materials of study [71]. The convective heat transfer depends on the quenched material [72] and cooling medium [73], and can be estimated from the thermal shock experiment itself, as demonstrated in [74] and later in [12] and [75]. Nevertheless, its value may be in a wide range, as reported in the literature, for example 10 – 100 kW/m²K in [42], 40 kW/m²K in [46], 50 kW/m²K in [49], 54.5 kW/m²K in [12] and lastly 70 kW/m²K in [68]. The value for this study was selected as 50 kW/m²K for comparative purposes.

Material properties were published previously [76] and are summarized in Table 1. The characteristic strength was determined on small discs made of both bulk A (effective surface area of $S \approx 0.4$ mm²) and bulk ZTA (effective surface area of $S \approx 1.5$ mm²) materials, using the ball-on-three-balls test [77] (biaxial bending strength). Square brackets in the Table 1 represent 90 % confidence interval for the Weibull modulus and the characteristic strength, respective. However, the specimens of study have a three orders of magnitude larger effective surface and thus the “equivalent” tensile strength was recalculated in the framework of Weibull statistics [56]. The characteristic strength of rods’ lateral surface in uniaxial tension can be recalculated from the biaxial bending using the Weibull scaling law as $\sigma_2 = \sigma_1 \sqrt[m]{S_1/S_2}$, which yields much smaller characteristic strength due to low Weibull modulus. Although ZTA has a higher bending strength than alumina, their strengths become comparable in tension [78]. We use characteristic strength in tension as tensile strength σ_c in our model [79]. The critical energy release rate, G_c , was calculated from the fracture toughness, K_{Ic} , and elastic moduli as $G_c = K_{Ic}^2 (1 - \nu^2)/E$.

2.2. Empirical observations of thermal shock cracks

Thermal shock tests were conducted on selected specimens of 3D-printed ZTA. The manufacturing process of the samples has been described elsewhere [70]. The ZTA rods were heated within a vertical tubular furnace (HTM Reetz GmbH, Berlin, Germany) to 20 °C below the desired maximum temperature by using a rate of 5 °C/min. Afterwards, the heating rate was changed to 2.5 °C/min until the maximum temperature (T_{max}) was achieved, followed by a holding time of approx. 15 min. Then, the rods were quenched into water at a temperature of $T_w \approx 20$ °C. Two temperature differences ($\Delta T_0 = T_{max} - T_w$) were selected, namely 250 °C and 400 °C, for the thermal shock experiments. Subsequently, the rods were treated with liquid dye penetrant (Diffu-Therm® red penetrant) for several minutes

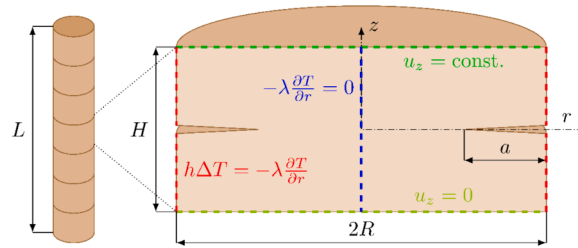


Fig. 3. Representative volume element for circumferential crack of depth a in a cylinder segment.

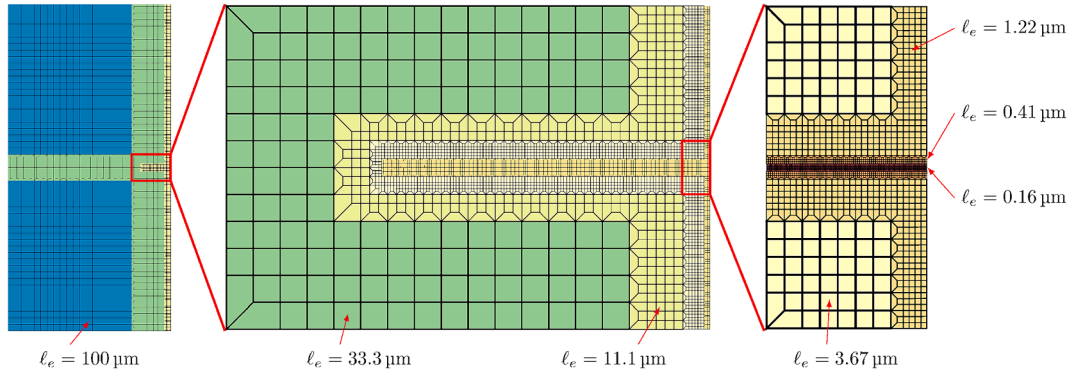


Fig. 4. Meridian plane of a RVE discretized by a mesh of 2D quadrilateral finite elements refined in crack vicinity. Largest elements (blue) have side length of $100 \mu\text{m}$ smallest elements (red) only $0.16 \mu\text{m}$.

and images of the crack patterns were taken using stereomicroscope (Olympus SZH10) with KL2500 LCD light source through the software (Stream motion, Olympus).

Fig. 2 shows the optical images of the non-shocked as well as thermally shocked ZTA rods at a ΔT_0 of $250 \text{ }^\circ\text{C}$ and $400 \text{ }^\circ\text{C}$, respectively. The first crack initiation on ZTA was found at ΔT_0 of $250 \text{ }^\circ\text{C}$, showing only a single circumferential crack along the rods surface (see Fig. 2b). We caution the reader that at the temperature difference ΔT_0 of $250 \text{ }^\circ\text{C}$ two out of the three specimens were not cracked, which indicates that the selected ΔT_0 is near to the critical temperature difference ΔT_c of the material. As comparison, the reference (non-shocked) specimen is depicted in Fig. 2a. At a temperature difference ΔT_0 of $400 \text{ }^\circ\text{C}$, which is significantly higher than the critical temperature difference, a rather dense crack pattern developed (Fig. 2c). These empirical observations are in agreement with the existing literature [1].

3. Crack initiation model

A slender ceramic rod of height $L = 50 \text{ mm}$ with a circular cross-section of radius $R = 2.5 \text{ mm}$ is depicted in Fig. 3. Due to the assumption of uniform crack spacing H , ring shape and size of cracks, the representative volume element (RVE) concept [49] is employed, which also exploits axial symmetry. The finite element method was used to simulate evolution of temperature, stress, and energy in a cylinder segment in which a single circumferential crack of depth a shall initiate.

After the rod is heated to a uniform temperature T_0 , it is rapidly cooled in the water at $20 \text{ }^\circ\text{C}$, the heat leaves through the surface causing temperature gradient in the body. Although the fall of specimens into the water is typically uncontrolled, we assume for simplicity that the heat flows uniformly through the whole lateral surface. The heat flow through basal surfaces causes complicated temperature and stress field near the bases, but does not influence the rest of the volume, and can be neglected in this study. Boundary conditions for transient thermal and subsequent static mechanical analysis are depicted in the Fig. 3.

3.1. Finite element model

Due to axial symmetry of the rod, only the meridian plane section was modelled. The RVE was discretized by a mesh of 8-node quadrilateral finite elements with quadratic shape functions and axisymmetric formulation (Ansys elements PLANE77 and PLANE183). Axisymmetric 2D model was compared with a 3D model made of 20-node hexahedral finite elements with quadratic shape functions (Ansys elements SOLID279 and SOLID186) and same results in temperature, deformation and stresses were obtained. The number of elements and nodes varies with the size of the RVE. For instance, the mesh of a 5 mm high RVE (depicted in the Fig. 4) has 79,146 elements and 247,487 nodes. After assessment of convergence of the stress and the strain energy, the largest elements had a side length of $100 \mu\text{m}$ and were refined along the prospective crack path down to $0.16 \mu\text{m}$ to achieve fine enough mesh to evaluate the

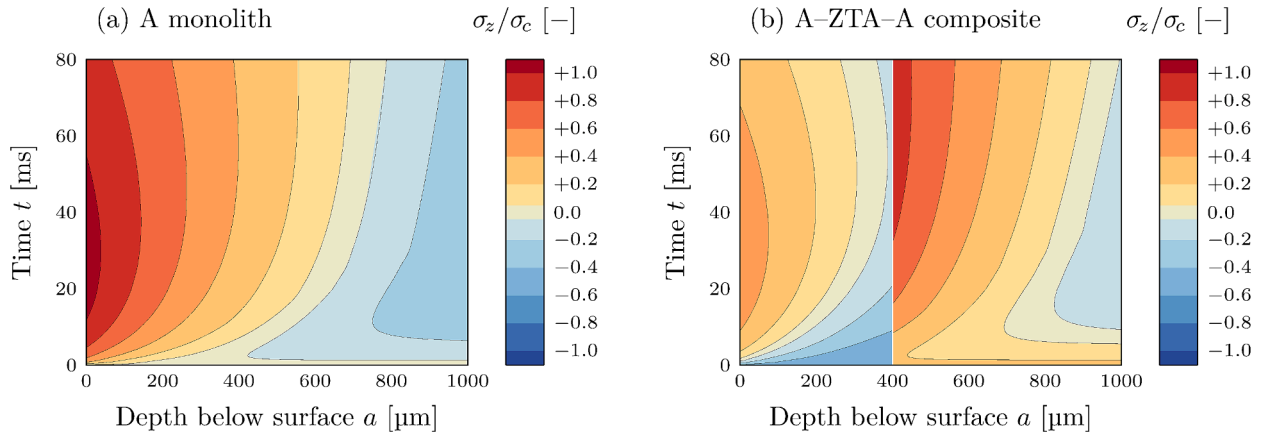


Fig. 5. Time evolution of the axial stress in the rod at $\Delta T_0 = 300^\circ\text{C}$ along radial direction plotted from the surface to the axis of symmetry for (a) monolithic A rod and for (b) bi-material rod with ZTA inside and alumina outside. Stress is normalized by the tensile strength of respective material.

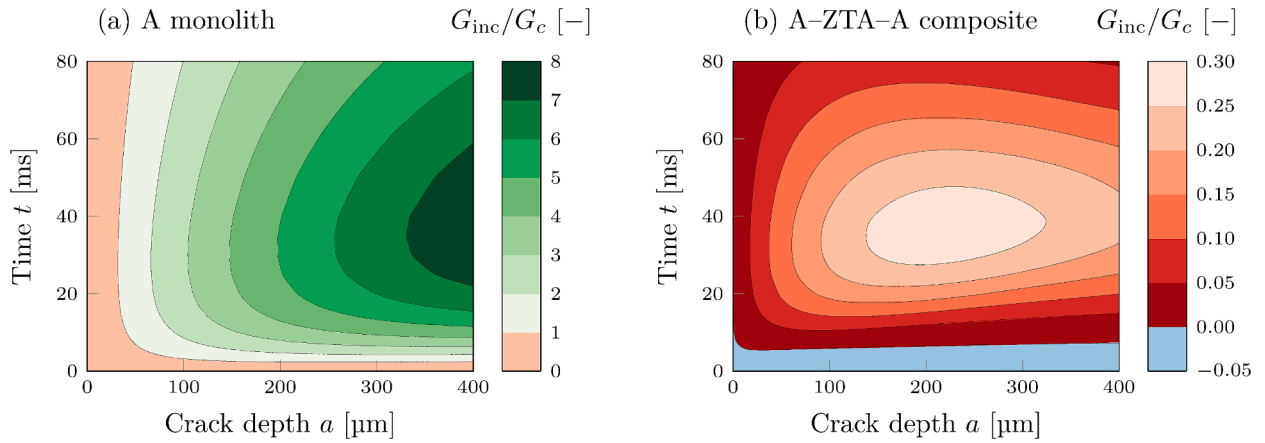


Fig. 6. Evolution of G_{inc} in time at $\Delta T_0 = 300^\circ\text{C}$ for a large crack spacing and various crack depths: (a) in A monolith and (b) in A-ZTA-A composite. Values are normalized by the critical value of the energy release rate G_c of alumina.

coupled criterion accurately, as recommended in [80]. Additionally, the mesh topology was not changed during calculations to avoid spurious energy variations. Crack closure in the presence of compressive residual stress was prevented by modelling contact between crack faces. Ansys elements TARGET169 and CONTA172 were created on both faces to establish a symmetric pair. Contact closure was detected using segment-to-segment formulation with pure Lagrange multiplier method to resolve contact penetration.

The calculations were performed as follows:

- In the first step, a transient thermal simulation of the cooling process during the first of 100 ms is performed without the presence of a crack. Automatic time stepping in Ansys with the initial time step $1\ \mu\text{s}$, minimal time step $0.1\ \mu\text{s}$ and maximal time step $0.5\ \text{ms}$ were chosen after assessing convergence conditions. The uniform temperature prior to contact with water starts decreasing rapidly at the surface but remains elevated in the depth for a certain time. This temperature gradient induces mismatch in thermal strains, responsible for crack nucleation.
- In the second step, stresses are evaluated within the same time range as the thermal analysis and without cracks. The temperature at a time between two time steps was linearly interpolated between them. The stress evolution is plotted as a function of time, as shown in Fig. 5. Stress component in the axial direction, i.e. the stress normal to crack faces, is plotted normalized by the calculated tensile strength of the alumina rod surface ($\sigma_c \approx 370\ \text{MPa}$). Before the quenching starts, the stress is zero everywhere in the monolithic case (Fig. 5a). However, in the bi-material case (Fig. 5b), although the uniform initial temperature is elevated, residual stresses from cooling down from the sintering are already present. Tensile stress rises rapidly at the surface of the rod while the inside of rod remains under the compression. In contrast to the monolithic case, the bi-material case starts with the surface under the compression due to alumina's smaller CTE, yet after certain time interval, tensile thermal stresses manage to overcome the compressive residual stresses.

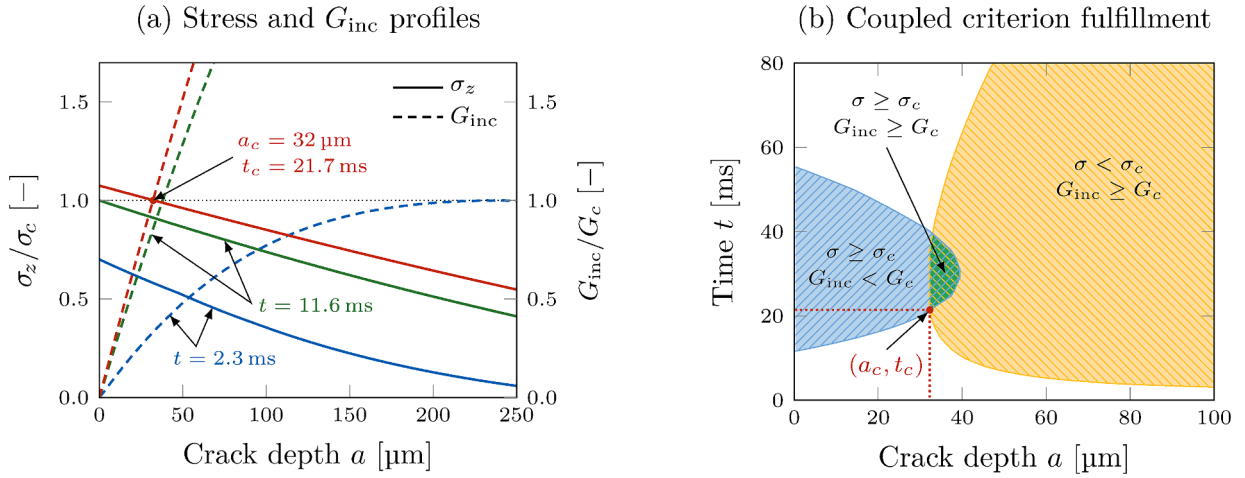


Fig. 7. Evaluation of the coupled criterion for an alumina rod at $\Delta T_0 = 350^\circ\text{C}$ with a single crack: (a) Stress (solid lines) and G_{inc} (dashed lines) profiles plotted at three distinct times (blue, green, and red colours) with respect to values of strength and critical energy release rate (dotted horizontal line). (b) Fulfilment of the stress criterion (blue region) and the incremental energy criterion (yellow region) simultaneously in the green region at various times and crack depths.

- In the third step, the strain energy Π of the whole body is calculated. First, the energy is evaluated in the presence of a large crack (up to 400 μm deep), which is then stepwise closed by merging coincident nodes on opposite crack faces to calculate energy $\Pi(A)$ with decreasing crack size A . The energy is evaluated at various sizes of smaller cracks until all nodes are merged and the crack is fully closed, corresponding to strain energy of the body without a crack, $\Pi(0)$. The area of the crack corresponds to a circular annulus and is calculated by Equation (3).

$$A = \pi R^2 - \pi(R - a)^2 \quad (3)$$

- Lastly, the incremental energy release rate G_{inc} is calculated in Equation (4) as the difference between a potential energy of the body without a crack, $\Pi(0)$, and the potential energy of the body with a crack, $\Pi(A)$, divided by the crack area A .

$$G_{\text{inc}} \stackrel{\text{def}}{=} - [\Pi(A) - \Pi(0)]/A \quad (4)$$

Fig. 6 illustrates G_{inc} (normalized by the critical energy release rate G_c) for a single crack, which grows independently of other neighbouring cracks, at various depths and times of thermal shock, with $\Delta T_0 = 300^\circ\text{C}$. In Fig. 6a, representing an alumina monolith, the red region (far left) indicates too short cracks and times to initiate any crack, whereas the green region (towards right) represents an energetically viable crack whose initiation surpasses the fracture toughness. The case of A-ZTA-A is shown in Fig. 6b for comparison under the same conditions. Due to the presence of compressive residual stress, G_{inc} is significantly lower. Here, red colours represent the non-fulfilment of the energy criterion, with lighter shades being closer to the fracture toughness. Furthermore, the blue region (bottom) represents a negative energy release rate, which is a consequence of compressive stresses that promptly close any potentially initiated crack prior to or at the beginning of the thermal shock.

3.2. Coupled criterion evaluation

For each calculated crack spacing and initial temperature difference we determine the minimum time at which the stress component σ_z exceeds the tensile strength and the incremental energy release rate surpasses the critical value of the energy release rate G_c . Fig. 7 represents an example of the coupled criterion evaluation at various times for a single crack in the whole specimen and an applied initial temperature difference $\Delta T_0 = 350^\circ\text{C}$.

Fig. 7a illustrates the evolution of stresses (σ_z) and incremental energy release rate (G_{inc}) for three given times after the thermal shock test, namely (i) 2.3 ms, (ii) 11.6 ms, and (iii) 21.7 ms. The solid lines represent the tensile stress from the surface to the bulk, being maximum at the surface and decaying in depth. The dashed lines represent G_{inc} for potential initial cracks of different depths. These lines are paired by colour that represents consecutive time after thermal shock start:

- o After 2.3 ms (the blue pair) it is energetically plausible to initiate large cracks approximately 250 μm long. However, the stress field along these potential cracks remains below the tensile strength σ_c of the material.
- o After 11.6 ms (the green pair) the developed stress reaches the material's strength but only near the surface, where the initiation of small cracks is still not energetically possible.

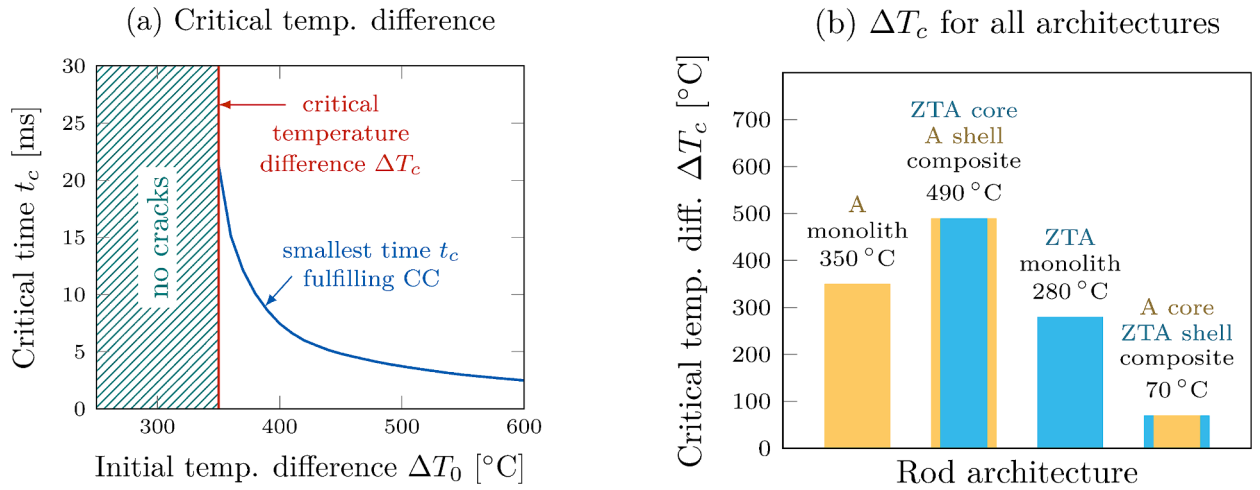


Fig. 8. Predicted critical temperature difference ΔT_c by the coupled criterion for (a) an alumina monolith with depicted smallest time t_c that fulfils the coupled criterion and (b) for all monoliths and core-shell composites.

- o After 21.7 ms (the red pair) a potential crack emerges, whose faces would be loaded by stresses exceeding the tensile strength of the material and simultaneously its initiation would be energetically possible. The intersection between this pair and the critical condition for stress and energy release rate is represented in Fig. 7a as the critical (initial) crack depth (a_c) at the critical time (t_c).

Fig. 7b illustrates three distinct regions representing the outcomes from the coupled criterion evaluation for thermal shock duration up to 80 ms:

- The blue region represents cracks which might have initiated according to the stress criterion ($\sigma \geq \sigma_c$) but are too small, thus lacking sufficient energy to initiate ($G_{inc} < G_c$).
- The yellow region represents cracks that are sufficiently long for an initiation from the energy point of view ($G_{inc} \geq G_c$), but without surpassing the tensile strength along the potential crack path ($\sigma < \sigma_c$) at any given time.
- The green region represents optimal crack depths that fulfil both conditions of the coupled criterion. The earliest time of initiation t_c and corresponding initial crack depth a_c are then determined and marked with a red dot. If such pair can be found, crack initiation takes place; otherwise, larger crack spacing, H , or higher initial temperature difference, ΔT_0 , should be chosen to facilitate crack formation.

4. Results and discussion

The thermal shock was simulated with an initial temperature difference ΔT_0 ranging from 50 °C to 700 °C, with steps of 50 °C. Stresses along the potential crack path and the strain energy in the whole body were evaluated at every 1 ms for the initial 20 ms period, followed by 5 ms intervals for the subsequent 20 ms and finally at every 10 ms for the remaining 60 ms. Results were linearly interpolated from these discrete times and simulated values of ΔT_0 .

4.1. Critical temperature difference

In Fig. 8a, the critical time t_c required for crack initiation (according to the coupled criterion) is plotted as a function of the initial thermal shock temperature difference, ΔT_0 . It is evident that the time required to fulfil the CC for the bulk alumina (A) material varies with the applied ΔT_0 . For sufficiently high initial temperature difference ($\Delta T_0 \geq \Delta T_c$), a minimum (critical) time exists at which at least one combination of crack depth and spacing fulfils the coupled criterion. However, as the ΔT_0 decreases, the time to reach critical conditions increases, as illustrated in Fig. 8a. At relatively high ΔT_0 , thermal shock cracks may initiate within few milliseconds. Below a certain initial temperature difference ΔT_0 , no combination of crack depth and spacing can fulfil the coupled criterion at any time. This threshold, defined as the critical temperature difference ΔT_c , represents a temperature difference below which thermal shock-induced cracks are not expected to initiate.

Fig. 8b illustrates the critical temperature difference ΔT_c determined using the coupled criterion for all four architectures depicted in Fig. 1. Monolithic rods are compared against composite bi-material rods. For the monolithic alumina rod (represented by the yellow left bar), no cracking is expected below the temperature difference $\Delta T_0 = 350$ °C, while for the ZTA monolithic rod (indicated by the blue bar) no cracking is anticipated below $\Delta T_0 = 280$ °C. In core-shell composite rods, where two materials are combined with a strong interface, residual stresses arise due to mismatches in thermal strains. The critical temperature difference for multi-material architectures may be influenced by the material properties and the distribution of residual stresses. An alumina shell over a ZTA core induces compressive residual stresses, reaching up to $\sigma_z^{res} \approx -280$ MPa at the room temperature. Conversely, a ZTA shell over an

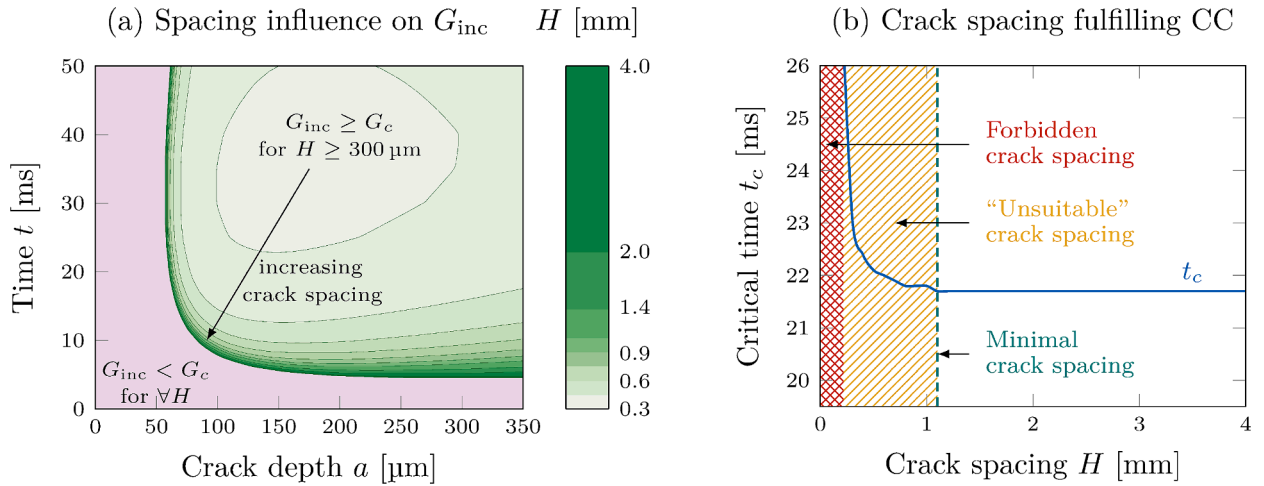


Fig. 9. Influence of the crack spacing H on (a) the incremental energy release rate G_{inc} and fulfilment of the energy criterion; (b) fulfilment of the coupled criterion.

alumina core results in tensile residual stress, with magnitude up to $\sigma_z^{res} \approx +270$ MPa at the room temperature. As a result, ΔT_c increases to 490 °C for the A-ZTA-A composite (the second bar from the left), whereas it decreases to 70 °C for the ZTA-A-ZTA composite (the fourth bar from the left).

It is important to highlight a potentially adverse consequence of combining two materials to enhance thermal shock resistance. While the alumina shell increases the surface's resistance to the thermal shock, it simultaneously subjects the core to a constant tension at the room temperature. This may facilitate the sub-critical growth of small defects, potentially leading to the core's fracture, leaving the shell without any protective residual stress. Potential mitigation involves the use of multiple layers, which (i) may decrease the residual stresses and (ii) would make the layers thinner, both providing a shielding effect [27]. Conversely, a ZTA shell becomes extremely vulnerable to the thermal shock due to presence of tensile residual stress. Moreover, when the ZTA shell is fractured, residual stresses within the core would relax, hence, the crack shielding effect would be lost if only a single shell was combined with the core. Therefore, it may be crucial to have multiple layers to maintain the mismatch strain and compressive residual stresses. The concept of designing bi-materials in a so-called "non-periodic" architecture [81] may be explored in the future to optimize the resistance to thermal shock crack initiation.

4.2. Spacing of cracks

The coupled criterion can also predict minimal crack spacing. We parametrically studied thermal shock cracking for various crack spacings and finally selected those which are energetically most convenient for crack formation. Fig. 9 shows an influence of crack spacing H on the incremental energy release rate G_{inc} and fulfilment of both the incremental energy criterion and the coupled criterion at $\Delta T_0 = 350$ °C. A decrease in crack spacing leads to a corresponding decrease in G_{inc} , even when the pre-cracking stress remains unchanged.

Fig. 9a shows two main regions indicating the fulfilment of the energy criterion: (i) where G_{inc} is lower than the fracture toughness, shown in the violet region (far left and bottom), and (ii) where G_{inc} is higher than fracture toughness represented by shades of green (upper and right region). In the violet region, no crack spacing fulfils the energy criterion, even in the case of a single crack initiating alone in the entire specimen. This is valid for (i) very short times, when the depth of tensile stress below the surface is too shallow and for (ii) very short cracks which would not propagate even according to the Griffith-Irwin condition, due to rapid decay of the stress along the prospective crack path. The green regions vary in size and position based on the spacing between cracks. The crack spacing must be at least 300 μm to exceed the fracture toughness at all. Spacing of 300 μm fulfils the energy criterion in the lightest green region, which would shrink to a point with a slight decrease in spacing and vanish with only a slightly smaller spacing. As the crack spacing increases, shorter cracks fulfil the energy criterion at earlier times.

The influence of crack spacing on the critical time required to fulfil the coupled criterion is depicted in Fig. 9b. The minimal crack spacing is marked by a green dashed vertical line at $H = 1.1$ mm. Above this threshold, all crack spacings may initiate at the same critical time, making them equally probable to occur. Crack spacings, smaller than this threshold, are highlighted by the area with a yellow pattern. Critical time in this region is longer, meaning that cracks with these spacings would only initiate after those with larger spacing, making the former less likely to be observed. Crack spacing below $H = 300 \mu\text{m}$ (highlighted by area with a red pattern) does not fulfil the coupled criterion at any time (it corresponds to the violet region in Fig. 9a) and should not be observed.

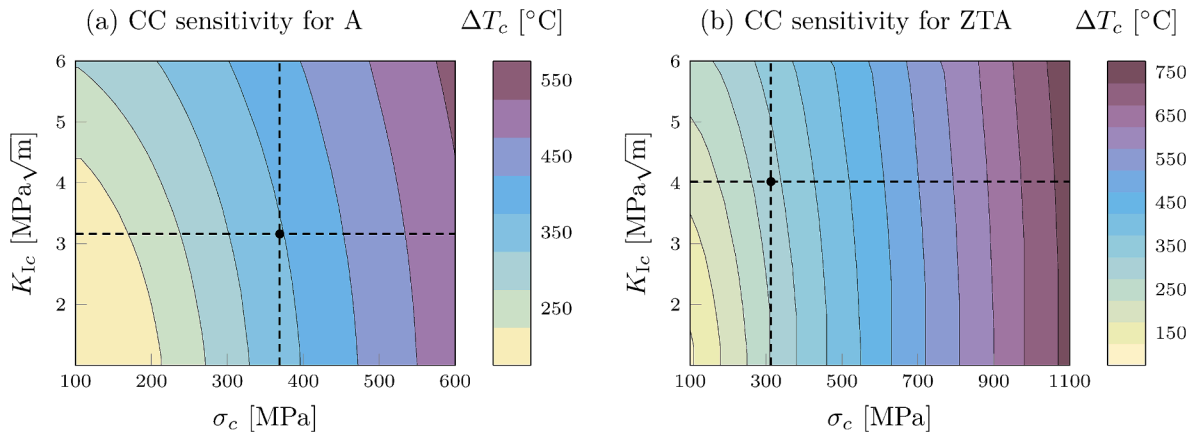


Fig. 10. Influence of the strength and toughness choice on the coupled criterion fulfilment for specimen with single crack made of (a) alumina and (b) ZTA material. Dashed lines represent initially chosen fracture parameters.

4.3. Effect of material properties on ΔT_c

It is necessary at this point to draw attention to the coupled criterion's sensitivity to the material's parameters that govern fracture behaviour— specifically, the tensile strength and the fracture toughness of materials. Evaluating the coupled criterion for (a) alumina and (b) ZTA monolithic rods with different σ_c and K_{Ic} values results in different predictions of ΔT_c , as illustrated in Fig. 10. Changes in ΔT_c are minimal with variation of the fracture toughness; property that can be experimentally measured with high accuracy in ceramics. In contrast, a slight change in the tensile strength of the material leads to significantly different ΔT_c . On one hand, this poses a challenge for reliable predictions; but on the other hand, it presents an opportunity to increase accuracy of determining the tensile strength. This potential arises from the important observation [4] that the thermal shock experiments with small-grain polycrystalline ceramics do not exhibit a scatter in the critical temperature difference. This aspect requires further attention but is beyond the scope of this work.

5. Summary and conclusions

This study focused on evaluating the impact of residual stresses on thermal shock resistance in ceramic materials, employing finite fracture mechanics to analyse crack initiation in both monolithic and bi-material rods composed of alumina (A) and zirconia-toughened alumina (ZTA). Our results revealed that surface compressive residual stresses in bi-material configurations can significantly enhance thermal shock resistance compared to monolithic counterparts, with a corresponding higher critical temperature difference required for crack initiation. The A-ZTA-A composite designed with -280 MPa of axial residual stress in the outer layers resulted in 140 °C higher critical temperature difference for thermal shock. We conclude that this raise is significant and further analysis of other layer thicknesses and other combinations of materials should be pursued.

The sensitivity of the thermal shock response to the tensile strength is demonstrated, highlighting the challenge in predicting crack initiation due to the significant impact of minor variations in the tensile strength. Conversely, fracture toughness showed a negligible influence on the critical temperature difference, suggesting a potential avenue for refining tensile strength predictions. We conclude that surfaces subjected to thermal shock should receive special attention to remove as many surface defects as possible since it is the strength that mainly governs the fracture under thermal shock.

Future research should further explore the optimization of the internal architecture of the multilayer (e.g. non-periodic designs) to leverage the protective effects of compressive residual stresses more effectively.

CRediT authorship contribution statement

Roman Papšík: Writing – original draft, Software, Methodology, Investigation, Formal analysis, Data curation. **Oldřich Ševeček:** Writing – review & editing, Supervision, Formal analysis. **Josef Schlacher:** Writing – review & editing, Resources, Investigation, Data curation. **Raúl Bermejo:** Writing – review & editing, Supervision, Project administration, Formal analysis, Conceptualization.

Declaration of competing interest

The authors declare that they have no known competing financial interests or personal relationships that could have appeared to influence the work reported in this paper.

Data availability

Data will be made available on request.

Acknowledgements

Funding for this research was provided by the European Research Council (ERC) excellent science grant “CERATEXT” through the Horizon 2020 program under contract 817615. The research was also supported by the project “Mechanical Engineering of Biological and Bio-inspired Systems”, funded as project No. CZ.02.01.01/00/22_008/0004634 by Programme Johannes Amos Comenius, call Excellent Research. We gratefully acknowledge Serkan Nohut (Lithoz GmbH) for providing the 3D-printed specimens for thermal shock testing.

References

- [1] Hasselman DPH. Strength behavior of polycrystalline alumina subjected to thermal shock. *J Am Ceram Soc* 1970;53:490–5.
- [2] Hasselman DPH. Unified theory of thermal shock fracture initiation and crack propagation in brittle ceramics. *J Am Ceram Soc* 1969;52:600–4.
- [3] Xu X, Sheng S, Yuan W, Lin Z. “Effect of grain size on thermal shock property of alumina ceramic”. *International Journal of Computational Materials Science and Engineering* 2016;5.
- [4] Gupta TK. Strength Degradation and Crack Propagation in Thermally Shocked Al₂O₃. *J Am Ceram Soc* 1972;55:249–53.
- [5] Coppola JA, Krohn DA, Hasselman DPH. Strength loss of brittle ceramics subjected to severe thermal shock. *J Am Ceram Soc* 1972;55:481.
- [6] Bahr HA, Balke H, Kuna M, Liesk H. Fracture analysis of a single edge cracked strip under thermal shock. *Theor Appl Fract Mech* 1987;8:33–9.
- [7] Bahr HA, Fischer G, Weiss HJ. Thermal-shock crack patterns explained by single and multiple crack propagation. *J Mater Sci* 1986;21:2716–20.
- [8] Xu X, Tian C, Sheng S, Lin Z, Song F. Characterization of thermal-shock cracks in ceramic bars. *Science China Physics, Mechanics & Astronomy* 2014;57:2205–8.
- [9] Liu Y, Wu X, Guo Q, Jiang C, Song F, Li J. Experiments and numerical simulations of thermal shock crack patterns in thin circular ceramic specimens. *Ceram Int* 2015;41:1107–14.
- [10] Bahr HA, Weiss HJ. Heuristic approach to thermal shock damage due to single and multiple crack growth. *Theor Appl Fract Mech* 1986;6:57–62.
- [11] Bahr HA, Weiss HJ, Maschke HG, Meissner F. Multiple crack propagation in a strip caused by thermal shock. *Theor Appl Fract Mech* 1988;10:219–26.
- [12] Jiang C, Wu X, Li J, Song F, Shao Y, Xu X, et al. A study of the mechanism of formation and numerical simulations of crack patterns in ceramics subjected to thermal shock. *Acta Mater* 2012;60:4540–50.
- [13] Shao Y, Song F, Liu B, Li W, Li L, Jiang C. Observation of ceramic cracking during quenching. *J Am Ceram Soc* 2017;100:520–3.
- [14] Shao Y, Liu B, Wang X, Li L, Wei J, Song F. Crack propagation speed in ceramic during quenching. *J Eur Ceram Soc* 2018;38:2879–85.
- [15] Bahr HA, Weiss HJ, Bahr U, Hofmann M, Fischer G, Lampenscherf S, et al. Scaling behavior of thermal shock crack patterns and tunneling cracks driven by cooling or drying. *J Mech Phys Solids* 2010;58:1411–21.
- [16] Shao Y, Xu X, Meng S, Bai G, Jiang C, Song F. Crack patterns in ceramic plates after quenching. *J Am Ceram Soc* 2010;93:3006–8.
- [17] Shao Y, Zhang Y, Xu X, Zhou Z, Li W, Liu B. Effect of Crack Pattern on the Residual Strength of Ceramics After Quenching. *J Am Ceram Soc* 2011;94:2804–7.
- [18] Hashin Z. Analysis of cracked laminates: a variational approach. *Mech Mater* 1985;4:121–36.
- [19] Weißgraeber P, Leguillon D, Becker W. A review of finite fracture mechanics. *Arch Appl Mech* 2016;86:375–401.
- [20] D. Leguillon, „Strength or toughness?“, *European Journal of Mechanics – A/Solids*, Bd. 21, pp. 61-72, 13 February 2002.
- [21] É. Martin, D. Leguillon and N. Carrère, „A coupled strength and toughness criterion for the prediction of the open hole tensile strength of a composite plate,“ *International Journal of Solids and Structures*, Bd. 49, pp. 3915-3922, 15 December 2012.
- [22] Martin É, Leguillon D, Catapano A, Carrère N. Prediction of interfacial debonding between stiff spherical particles and a soft matrix with the coupled criterion. *Theor Appl Fract Mech* 2020;109.
- [23] Mantić V. Interface crack onset at a circular cylindrical inclusion under a remote transverse tension. *Int J Solids Struct* 2009;46:1287–304.
- [24] Doitrand A, Fagiano C, Carrère N, Chiaruttini V, Hirsekorn M. Damage onset modeling in woven composites based on a coupled stress and energy criterion. *Engng Fract Mech* 2017;169:189–200.
- [25] García I, Mantić V, Blázquez A, París F. Transverse crack onset and growth in cross-ply laminates under tension. *Int J Solids Struct* 2014;51:3844–56.
- [26] M. Kashtalyan, I. García García und V. Mantić, „Coupled stress and energy criterion for multiple matrix cracking in cross-ply composite laminates,“ *International Journal of Solids and Structures*, Bde. 1 von %2139-140, pp. 189-199, 15 May 2018.
- [27] Papsík R, Ševeček O, Hofer A-K, Králeva I, Kreith J, Bermejo R. Prediction of edge and tunnelling crack formation in layered ceramics using a stress-energy fracture criterion. *J Eur Ceram Soc* 2023;43:2928–34.
- [28] D. Leguillon, É. Martin, O. Ševeček und R. Bermejo, „Application of the coupled stress-energy criterion to predict the fracture behaviour of layered ceramics designed with internal compressive stresses,“ *European Journal of Mechanics – A/Solids*, Bd. 54, pp. 94-104, June 2015.
- [29] Leguillon D, Martin É. Prediction of multi-cracking in sub-micron films using the coupled criterion. *Int J Fract* 2018;209:187–202.
- [30] D. Leguillon, J. Li und É. Martin, „Multi-cracking in brittle thin layers and coatings using a FFM model,“ *European Journal of Mechanics – A/Solids*, Bd. 63, pp. 14-21, May 2017.
- [31] Strobl M, Dowgiało P, Seelig T. Analysis of Hertzian indentation fracture in the framework of finite fracture mechanics. *Int J Fract* 2017;206:67–79.
- [32] Hahn J, Becker W. Determination of Strength and Fracture Toughness from Indentation Tests in the Framework of Finite Fracture Mechanics. in *Computational and Experimental Simulations in Engineering*. 2021.
- [33] Papsík R, Ševeček O, Martin É, Bermejo R. Prediction of ring crack initiation in ceramics and glasses using a stress-energy fracture criterion. *Journal of the American Ceramic Society*, Nr 2023;106:4329–42.
- [34] Doitrand A, Molnár G, Leguillon D, Martin E, Carrère N. “Dynamic crack initiation assessment with the coupled criterion”. *European Journal of Mechanics – A/ Solids* 2022;93.
- [35] Chao Correias A, Cornetti P, Corrado M, Sapora A. „Finite Fracture Mechanics extension to dynamic loading scenarios. “ *International Journal of Fracture* 2022; 239.
- [36] Cornetti P, Sapora A. Penny-shaped cracks by Finite Fracture Mechanics. *Int J Fract* 2019;219:153–9.
- [37] A. Doitrand, R. Henry, J. Chevalier und S. Meille, „Revisiting the strength of micron-scale ceramic platelets,“ *Journal of the American Ceramic Society*, pp. 1-10, 08 April 2020.
- [38] Doitrand A, Henry R, Saad H, Sylvain D, Meille S. Determination of interface fracture properties by micro- and macro-scale experiments in nacre-like alumina. *J Mech Phys Solids* 2020;145:1–14.
- [39] Jiménez-Alfaro S, Leguillon D. Finite fracture Mechanics at the micro-scale. *Engng Fract Mech* 2021;258.
- [40] Duminy T, Henry R, Adrien J, Doitrand A, Meille S. Anisotropic fracture in nacre-like alumina. *Theor Appl Fract Mech* 2023;123.
- [41] A. Doitrand, T. Duminy, H. Girard und X. Chen, “A review of the coupled criterion”, 2023.
- [42] Li J, Song F, Jiang C. Direct numerical simulations on crack formation in ceramic materials under thermal shock by using a non-local fracture model. *J Eur Ceram Soc* 2013;33:2677–87.
- [43] Sicsic P, Marigo J-J, Maurini C. Initiation of a periodic array of cracks in the thermal shock problem. *J Mech Phys Solids* 2014;63:256–84.

- [44] Tang S, Zhang H, Tang C, Liu H. Numerical model for the cracking behavior of heterogeneous brittle solids subjected to thermal shock. *Int J Solids Struct* 2016; 80:520–31.
- [45] Giannakeas IN, Papathanasiou TK, Bahai H. Simulation of thermal shock cracking in ceramics using bond-based peridynamics and FEM. *J Eur Ceram Soc* 2018; 38:3037–48.
- [46] Wang Y, Zhou X, Zhang T. Size effect of thermal shock crack patterns in ceramics. *Mech Mater* 2019;137:103133.
- [47] Storm J, Yin B, Kaliske M. The concept of Representative Crack Elements (RCE) for phase-field fracture: transient thermo-mechanics. *Comput Mech* 2022;69: 1165–76.
- [48] Jesch-Weigel N, Zielke R, Hofmann M, Wallmersperger T. Analysis of 3D crack patterns in a free plate caused by thermal shock using FEM-bifurcation. *Int J Fract* 2023;238.
- [49] L. F. Faria Ricardo, D. Leguillon, G. Parry und A. Doitrand, „Modeling the thermal shock induced cracking in ceramics,“ *Journal of the European Ceramic Society*, Bd. 40, pp. 1513-1521, April 2020.
- [50] Li D, Wang R, Wang X, Li W. „Simulation of the thermal shock cracking behaviors of ceramics under water quenching for 3-dimension conditions. “ *European Journal of Mechanics – A/Solids* 2020;84.
- [51] D. Li, Y. Pang, T. Lu, Z. Liu and S. Chen, “Numerical Analysis of Thermal Shock Cracking Behaviors of Ceramics Based on the Force-Heat Equivalence Energy Density Principle,” *Frontiers in Materials*, vol. 8, January 2022.
- [52] Chu D, Li X, Liu Z. Study the dynamic crack path in brittle material under thermal shock loading by phase field modeling. *Int J Fract* 2017;208:115–30.
- [53] Wang T, Ye X, Liu Z, Liu X, Chu D, Zhuang Z. A phase-field model of thermo-elastic coupled brittle fracture with explicit time integration. *Comput Mech* 2020; 65:1305–21.
- [54] Mandal TK, Nguyen VP, Wu J-Y, Nguyen-Thanh C, de Vaucorbeil A. Fracture of thermo-elastic solids. *Comput Methods Appl Mech Engng* 2021;376.
- [55] Li D, Li P, Li W, Li W, Zhou K. Three-dimensional phase-field modeling of temperature-dependent thermal shock-induced fracture in ceramic materials. *Engng Fract Mech* 2022;268.
- [56] Weibull W. A statistical distribution function of wide applicability. *ASME Journal of applied mechanics* 1951;18:293–7.
- [57] Danzer R, Lube T, Supancic P, Damani R. „Fracture of Ceramics, “ in *Ceramics Science and Technology*. John Wiley & Sons Ltd 2013:529–75.
- [58] A. Brückner-Foit, E. Diegele, P. Hülsmeier, U. Rettig und C. Hohmann, „Prediction of the Failure Probability of High Strength Ceramics Subject to Thermal Shock Loading,“ in 26th Annual Conference on Composites, Advanced Ceramics, Materials, and Structures: A: Ceramic Engineering and Science Proceedings, 2002.
- [59] Matsuda S. Fracture characteristics of silicon nitride ceramic ball subjected to thermal shock. *J Mater Sci* 2016;51:5502–13.
- [60] Lu TJ, Fleck NA. The thermal shock resistance of solids. *Acta Mater* December 1998;46:4755–68.
- [61] Collin MIK, Rowcliffe DJ. Analysis and prediction of thermal shock in brittle materials. *Acta Mater* 2000;48:1655–65.
- [62] Nordberg ME, Mochel EL, Garfinkel HM, Olcott JS. Strengthening by Ion Exchange. *J Am Ceram Soc* 1964;47:215–9.
- [63] J. Schlacher, A. Jabr, A.-K. Hofer and R. Bermejo, “Contact damage tolerance of alumina-based layered ceramics with tailored microstructures,” *Journal of the American Ceramic Society*, pp. 1-13, June 2022.
- [64] R. Papišik, O. Ševeček, ě. Martin und R. Bermejo, „Prediction of ring crack initiation in ceramics and glasses using a stress-energy fracture criterion,“ *Journal of the American Ceramic Society*, Nr. 106, pp. 4329-4342, 13 December 2022.
- [65] Vandepierre LJ, Kristofferson A, Carlström E, Clegg WJ. Thermal Shock of Layered Ceramic Structures with Crack-Deflecting Interfaces. *J Am Ceram Soc* 2001; 84:104–10.
- [66] Bermejo R, Llanes L, Anglada M, Supancic P, Lube T. Thermal Shock Behavior of an Al₂O₃/ZrO₂ Multilayered Ceramic with Residual Stresses due to Phase Transformations. *Key Engng Mater* 2005;290:191–8.
- [67] Bermejo R, Torres Y, Sánchez-Herencia AJ, Baudín C, Anglada M, Llanes LM. Fracture behaviour of an Al₂O₃-ZrO₂ multi-layered ceramic with residual stresses due to phase transformations*. *Fatigue Fract Engng Mater Struct* 2006;29:71–8.
- [68] Bermejo R, Supancic P, Lube T. Geometry Effect on the Thermal Shock Response of Al₂O₃/ZrO₂ Multilayered Ceramics. *Key Engng Mater* 2007;333:251–4.
- [69] Y. Pang, D. Li, X. Li, R. Wang and X. Ao, “Phase-Field Simulation of Temperature-Dependent Thermal Shock Fracture of Al₂O₃/ZrO₂ Multilayer Ceramics with Phase Transition Residual Stress,” *Materials*, vol. 16, January 2023.
- [70] Schlacher J, Geier S, Schwentenwein M, Bermejo R. Towards 3D-printed alumina-based multi-material components with enhanced thermal shock resistance. *J Eur Ceram Soc* 2024;44:2294–303.
- [71] Chlup Z, Hadraba H, Drdlík D, Maca K, Dlouhý I, Bermejo R. On the determination of the stress-free temperature for alumina–zirconia multilayer structures. *Ceram Int* 2014;40:5787–93.
- [72] Kim Y, Lee WJ, Case ED. The measurement of the surface heat transfer coefficient for ceramics quenched into a water bath. *Mater Sci Engng A* 1991;145:7–11.
- [73] Lee WJ, Kim Y, Case ED. The effect of quenching media on the heat transfer coefficient of polycrystalline alumina. *J Mater Sci* 1993;28:2079–83.
- [74] E. D. Case, „Heat Transfer Coefficient Estimation from Thermal Shock Data,“ in 26th Annual Conference on Composites, Advanced Ceramics, Materials, and Structures: A: Ceramic Engineering and Science Proceedings, 2002.
- [75] Zhou Z, Song F, Shao Y, Meng S, Jiang C, Li J. Characteristics of the surface heat transfer coefficient for Al₂O₃ ceramic in water quench. *J Eur Ceram Soc* 2012; 32:3029–34.
- [76] J. Schlacher, A.-K. Hofer, S. Geier, I. Kraveva, R. Papišik, M. Schwentenwein and R. Bermejo, “Additive manufacturing of high-strength alumina through a multi-material approach,” *Open Ceramics*, vol. 5, March 2021.
- [77] Börger A, Supancic P, Danzer R. The ball on three balls test for strength testing of brittle discs. *J Eur Ceram Soc* 2002;22:1425–36.
- [78] Leguillon D, Martin ě, Lafarie-Frenot M-C. Flexural vs. tensile strength in brittle materials. *Comptes Rendus Mécanique* 2015;343:275–81.
- [79] Leguillon D, Martin ě, Ševeček O, Bermejo R. What is the tensile strength of a ceramic to be used in numerical models for predicting crack initiation? *Int J Fract* 2018;212:89–103.
- [80] Doitrand A, Martin E, Leguillon D. Numerical implementation of the coupled criterion. *Finite Elem Anal Des* 2020;168:1–11.
- [81] Bermejo R. Toward seashells under stress. *J Eur Ceram Soc* 2017;37:3823–39.